



## Transport effects on the vertical distribution of tropospheric ozone over western India

Shyam Lal, S. Venkataramani, Naveen Chandra, Owen R. Cooper, Jérôme Brioude, Manish Naja

### ► To cite this version:

Shyam Lal, S. Venkataramani, Naveen Chandra, Owen R. Cooper, Jérôme Brioude, et al.. Transport effects on the vertical distribution of tropospheric ozone over western India. *Journal of Geophysical Research: Atmospheres*, 2014, 119 (16), pp.10012-10026. 10.1002/2014JD021854 . hal-01069991

**HAL Id: hal-01069991**

**<https://hal.science/hal-01069991>**

Submitted on 30 Sep 2014

**HAL** is a multi-disciplinary open access archive for the deposit and dissemination of scientific research documents, whether they are published or not. The documents may come from teaching and research institutions in France or abroad, or from public or private research centers.

L'archive ouverte pluridisciplinaire **HAL**, est destinée au dépôt et à la diffusion de documents scientifiques de niveau recherche, publiés ou non, émanant des établissements d'enseignement et de recherche français ou étrangers, des laboratoires publics ou privés.

**Transport effects on the vertical distribution of tropospheric ozone over western India.**

S. Lal<sup>1\*</sup>, S. Venkataramani<sup>1</sup>, N. Chandra<sup>1</sup>

O. R. Cooper<sup>2,3</sup> and J. Brioude<sup>2,3,4</sup>

M. Naja<sup>5</sup>

<sup>1</sup>Physical Research Laboratory, Navrangpura Ahmedabad, India

<sup>2</sup>Cooperative Institute for Research in Environmental Sciences, University of Colorado,  
Boulder, USA

<sup>3</sup>NOAA Earth System Research Laboratory, Boulder, USA

<sup>4</sup>Laboratoire de l'Atmosphere et des Cyclones, UMR8105, CNRS-Meteo France-Universite,  
La Reunion, La Reunion, France

<sup>5</sup>Aryabhatta Research Institute of Observational Sciences, Nainital, India

\* Corresponding author

## **Abstract**

In situ tropospheric ozone measurements by balloon borne electrochemical concentration cell (ECC) sensors above Ahmedabad in western India from May 2003 to July 2007 are presented, along with an analysis of the transport processes responsible for the observed vertical ozone distribution. This analysis is supported by 12-day back trajectory calculations using the FLEXPART Lagrangian particle dispersion model. Lowest ozone (~20 ppbv) is observed near the surface during September at the end of the Asian summer monsoon season. Average mid-tropospheric (5-10 km above sea level) ozone is greatest (70-75 ppbv) during April-June and lowest (40-50 ppbv) during winter. Ozone variability is greatest in the upper troposphere with higher ozone during March-May. The FLEXPART retroplume results show that the free tropospheric vertical ozone distribution above this location is affected by long-range transport from the direction of North Africa and North America. Ozone levels are also affected by transport from the stratosphere particularly during March-April. The lower tropospheric (<3 km) ozone distribution during the Asian summer monsoon is affected by transport from the Indian Ocean via the east coast of Africa and the Arabian Sea. Influence from deep convection in the upper troposphere confined over central Asia has been simulated by FLEXPART. Lower ozone levels are observed during August-November than in any other season at 10-14 km above sea level. These in situ observations are in contrast to other studies based on satellite data which show that the lowest ozone values at these altitudes occur during the Asian summer monsoon.

## **1. Introduction**

Ozone in the troposphere plays crucial roles as an oxidant and as a greenhouse gas. It is the major source of the highly reactive OH radicals in the troposphere, which control oxidation processes as well as act as a cleaning agent by controlling the abundance of many trace gases,

particularly hydrocarbons [Monks et al., 2009]. Ozone traps the outgoing long-wave radiation at 9.6  $\mu\text{m}$ , and its contribution to radiative forcing is significant next to  $\text{CO}_2$  and  $\text{CH}_4$  [Gauss et al., 2003; Stevenson et al., 2012; IPCC, 2013]. The efficiency of this radiative forcing is greater at higher altitudes in the troposphere [Lacis et al., 1990; Gauss et al., 2003]. Ozone in the troposphere is also a pollutant that impacts air quality [The Royal Society, 2008; Ravishankara et al., 2012].

Ozone in the troposphere is either transported from the stratosphere or produced photochemically from pollutants emitted by anthropogenic and natural processes [Crutzen, 1995]. The first source is mostly dominant in the upper troposphere while the latter plays a major role in the lower troposphere. The lifetime of ozone varies from hours near the surface to months in the free troposphere. Since its lifetime is high in the mid- and upper troposphere, ozone (and some of its precursors) can be transported over long distances [Lelieveld et al., 2002, Liu et al., 2003; Lawrence and Lelieveld, 2010; Dentener et al., 2011]. Tropospheric ozone above the US is affected by south and east Asian anthropogenic emissions due to the prevailing westerly winds at mid-latitudes [Cooper et al., 2005a, 2010; Lin et al., 2012]. However, Asia is also influenced by European emissions [Wild et al., 2004; Naja and Akimoto, 2004]. Particularly relevant to this analysis, a study of ozone profiles in the lower troposphere shows that Ahmedabad in western India is affected by transport from Southern Europe and North Africa [Srivastava et al., 2012].

South and East Asian countries are experiencing strong industrial and economic growth leading to increasing emissions of pollutants, many of which are ozone precursors [Akimoto, 2003; Streets et al., 2003; Gurjar et al., 2004; Lal et al., 2004; Olivier et al., 2005; Ohara et al., 2007]. Because the tropical regions of Asia are strongly affected by deep convection [Emanuel,

1994] the region's ozone and ozone precursors can be lofted to the mid- and upper troposphere, with subsequent advection across great distances [Kley *et al.*, 1997; Kar *et al.*, 2004; Folkins and Martin, 2005]. During the last decade, enhanced pollution in the upper troposphere has been observed over Asia and the Middle East due to wide-spread deep convection during the summer monsoon period. The polluted convective outflow can be confined over this region by the strong anticyclonic circulation associated with the Asian summer monsoon [Gettelman *et al.*, 2004; Randel and Park, 2006; Randel *et al.*, 2010; Park *et al.*, 2007; Worden *et al.*, 2009; Liu *et al.*, 2009, 2011; Barret *et al.*, 2011].

India is a developing country located in the tropics and sub-tropics with over one billion citizens. Hence, the atmosphere over this region is strongly impacted by increasing emissions of pollutants due to anthropogenic activity, along with intense sunlight and high water vapour content. However, studies related to tropospheric ozone are very limited for the Indian region despite its importance for the northern hemisphere budgets of ozone and particulate matter [Lawrence and Lelieveld, 2010], with many of these studies based on satellite data [Fishman *et al.*, 2003; Saraf and Beig, 2004; Beig and Singh, 2007; Fadnavis *et al.*, 2010]. Here we present an analysis of tropospheric ozone based on in situ ozonesonde observations from May 2003 to July 2007 to improve the scientific community's understanding of the ozone distribution above western India and the transport processes that modulate its abundance.

## **2. Location and meteorology**

Ahmedabad (23.03°N, 72.54°E, 50 m amsl) (See Figure 1) is an urban centre in central west India, with a population of 5.6 million that has increased by about 20% in the last decade [http://www.censusindia.gov.in]. The Thar Desert is located to the north-west (about 500 km) and the Arabian Sea to the south-west with the closest shores being 100 km to the south and

400 km to the west. Physical Research Laboratory (PRL), where the ozonesondes were launched, is located on the western side of the city. Textile mills and pharmaceutical production facilities are located in and around the city with most industries in the eastern and northern regions, about 15-20 km from PRL. In addition, a 400 MW coal fired power plant is located approximately 10 km to the northeast. Ahmedabad has a large number (about 2.5 million) of automobiles, which are increasing at the rate of about 10% per year.

Ahmedabad has a hot semi-arid climate. The climate is dry except during the summer monsoon season. The weather is hot from April to June, while winds during December-February bring milder conditions. The monthly average surface temperature is in the range of 28 °C to 35 °C during summer and 20 °C to 25 °C during the winter months of November to February. The southwest Asian summer monsoon produces a humid climate from mid-June to mid-September with an average annual rainfall of about 750 mm. Most rainfall over Ahmedabad occurs during July (~43%) and August (~27%).

The average wind patterns based on NCEP reanalysis data for December-January- February (DJF), March-April-May (MAM), June-July-August (JJA) and September-October-November (SON) on the 925, 500 and 200 hPa surfaces are shown in Figure 1. The winds over Ahmedabad at 925 hPa are north-easterly during winter (DJF), westerly during spring (MAM), south westerly during the summer monsoon (JJA) and north-westerly during autumn (SON). The streamlines at 500 hPa are south-westerly during DJF, westerly during MAM, north-easterly during JJA and again westerly during SON. At 200 hPa, the winds are stronger and south-westerly during DJF, westerly during MAM and again south-westerly during SON. However, the winds are easterly during the summer monsoon months with an anticyclone pattern centred over the Himalaya and extending to the Middle East.

### 3. Techniques

#### 3.1 Ozone and meteorological soundings

Vertical profiles of ozone, pressure, humidity and temperature were measured using balloon borne ozonesondes coupled to radiosondes. Each ozonesonde consists of a Teflon pump, an ozone sensing electrochemical concentration cell (ECC) [Komhyr and Harris, 1971] and an electronic interface board. The ECC is comprised of Teflon cathode and anode chambers containing platinum electrodes immersed in KI solutions of two different concentrations thereby providing a potential difference to collect the electrons produced in the cathode chamber from the reaction between the KI solution and ozone present in the ambient atmosphere. Its accuracy is  $\pm 5$ -10% up to 30 km altitude [Smit *et al.*, 2007]. The Vaisala RS-80 radiosonde consists of capacitance based temperature, humidity and pressure sensors. The temperature and pressure sensors have accuracies below 20 km of  $\pm 0.3$  °C, and  $\pm 0.5$  hPa, respectively. The heights are calculated based on the observed pressure and are above mean sea level (AMSL). However, the humidity sensor has an accuracy of about  $\pm 2$ % near the ground which decreases to  $\pm 15$ -30% in the 5-15 km altitude range [Kley *et al.*, 1997].

Balloon soundings carrying an ozonesonde and a radiosonde were made from the terrace of PRL once every two weeks between 9:30-10:30 AM IST (UTC+ 5.5 hrs). Some of these sondes also carried a GPS, which provided winds in addition to the position information. The exact launch time depended on clearance from the Air Traffic Control of the local airport. The first flight was made on 7 May, 2003 and the last on 11 July, 2007. There were breaks in between due to technical problems or due to other campaigns. A total of 83 ozonesondes were launched during this period. The balloons reached a maximum altitude of 30 to 33 km with an average ascent rate of about  $250 \text{ ms}^{-1}$ . The instruments fell mostly within 150 km around the

launch site and some of the ozone sensors were recovered and were flown again after proper cleaning, charging and testing.

Typical vertical distributions of air temperature, relative humidity and ozone are shown in Figure 2. The humidity profile is shown up to about 20 km but errors are large above 10 km. The figure shows structures in the humidity profile and often corresponding changes in temperature. The ozone profile also shows variability sometimes linked to changes in humidity and temperature. The ozone partial pressure increases rapidly around 18 km, peaks around 28 km, and decreases above this altitude.

### **3.2. Lagrangian Dispersion Model**

The FLEXPART Lagrangian particle dispersion model (version 8.1) [Stohl *et al.*, 2005] was used to simulate the 12-day transport history of each ozonesonde profile at 200 m intervals. The model calculates the trajectories of a multitude of particles and was driven by ECMWF ERA-interim global wind fields, with a temporal resolution of 6 h (analyses at 0000, 0600, 1200, and 1800 UTC), horizontal resolution of  $0.7^\circ \times 0.7^\circ$ , and 37 pressure levels. Particles are transported both by the resolved winds and parameterized sub-grid motions, including a vertical deep convection scheme.

To determine the transport history of each ozone measurement, a retroplume was calculated (see Cooper *et al.*, [2005a, b] for a detailed illustration of the method) consisting of 40,000 back trajectory particles released from a box surrounding the location and time of each measurement (1 hour duration; 10 km x 10 km x 200 m box) and advected backwards in time over a 12-day period. Retroplume distributions were output in 1-day intervals on a  $2^\circ \times 2^\circ$  degree output grid covering the globe, with a  $0.5^\circ \times 0.5^\circ$  nested grid over India. FLEXPART



176 outputs the retroplumes in units of  $\text{s kg}^{-1} \text{m}^3$ , which is the residence time of the plume per grid  
177 cell divided by the air density. The residence of each retroplume is calculated for the 300 m  
178 layer of the atmosphere adjacent to the Earth's surface where the air would pick up surface  
179 emissions (known as the footprint layer). For simplicity this specific volume weighted  
180 residence time is hereafter referred to as the retroplume residence time.

181  
182 The dispersion of a retroplume backwards in time indicates the likely source regions of the  
183 ozone precursors (or stratospheric intrusions) that contributed to the measured ozone, but over  
184 the previous 12 days. This is especially true of the so-called footprint layer which is the 300 m  
185 layer adjacent to the Earth's surface. For plumes passing through this layer the residence time  
186 of the back trajectory particles is folded with an anthropogenic  $\text{NO}_x$  emission inventory to  
187 quantify the amount of anthropogenic  $\text{NO}_x$  emitted into the air mass represented by the  
188 retroplume [Stohl *et al.*, 2003]. The  $\text{NO}_x$  emission inventory used in this study is the  
189 EDGARv4.1 2005 annual data set, which estimates anthropogenic  $\text{NO}_x$  emissions on land  
190 [Olivier *et al.*, 2005]. International shipping  $\text{NO}_x$  emissions are from the University of  
191 Delaware 2001 inventory [Corbett and Koehler, 2003]. Monthly biomass burning emissions  
192 were provided by the Global Fire Emission Database (GFED) version 3  
193 (<http://www.globalfiredata.org>) [van der Werf *et al.*, 2010]. With this technique the quantity  
194 of  $\text{NO}_x$  emitted into each retroplume from several source regions (India, Southeast Asia, China,  
195 Japan-Korea, Central Asia, Middle East, Africa, Europe, North America and South America)  
196 was tabulated. The  $\text{NO}_x$  tracer has no chemical or depositional removal processes and is treated  
197 as a passive tracer. The ECMWF ERA-Interim analyses contain stratospheric ozone values  
198 above the tropopause. We use these gridded values to calculate the quantity of ozone  
199 transported from the stratosphere to the location where a retroplume is released. This method  
200 involves tagging all retroplume back trajectory particles that originated in the stratosphere and

scaling the mass of each particle by the ozone value at its highest altitude in the lower stratosphere. The accuracy of the stratospheric ozone tracer was also assessed using 260 ozonesonde profiles above the USA during summer 2004 [Cooper et al., 2005b, 2006]. The result is an upper limit of the estimated stratospheric ozone that was directly transported from the stratosphere to a retroplume release point over the previous 12 days.

## **4. Results and discussions**

### **4.1 Temperature and humidity variations**

The observed average air temperature in the troposphere is shown in Figures 3a and 3 c. The average seasonal temperature profiles show minimum surface temperatures of about 20 °C in winter (DJF) at the time of morning balloon launches (9:30 – 10:30 am). Winter temperatures are lower than in all other seasons up to about 15 km. The highest average seasonal surface temperature (about 30 °C) is observed in spring (MAM). But at 3-15 km, spring temperatures are lower than during JJA and SON. The highest temperatures at 3-15 km are observed during the summer monsoon season (JJA). The lapse rates vary widely below about 4 km in the planetary boundary layer but between 4 km and 15 km, they are mostly in the range of -8 to -5 °C/km. The tropopause is observed to be in the 16-18 km range.

Relative humidity varies widely with altitude and from month to month and is at a maximum during the summer monsoon (JJA) and lower during winter and spring (Figures 3b and c). The average monthly minimum at the surface occurs in November (~25%) and the maximum occurs in July (~69%). The greatest values extend up to about 10 km during the peak monsoon month of July. Occasionally, higher relative humidity is also observed in December/January due to the winter monsoon.

## 4.2 Ozone distribution in the troposphere

The average seasonal profiles of ozone mixing ratios are shown in Figure 4a. Ozone increases rapidly with altitude in the lower troposphere (below about 1 km height) during winter (DJF). Average ozone is about 28 ppbv near the surface but increases to about 56 ppbv near 1 km. This could be due to a shallow boundary layer during this season and loss near the surface due to dry deposition or destruction by NO. Above 1 km, ozone decreases to about 45 ppbv at 3.5 km; above this altitude ozone increases slowly throughout the entire troposphere. In the middle troposphere (4 to 10 km, height), average ozone is highest in spring (MAM) and the summer monsoon (JJA) seasons and lowest in the winter season (DJF). Ozone is lowest (~18 ppbv) during the monsoon season (JJA) near the surface and remains low below 3 km. However, at 7 to 9 km ozone is slightly greater (~ 66 ppbv) in JJA than during MAM. Ozone during autumn (SON) is similar to spring below 3.5 km but it is lower than all other seasons between 9 and 16 km. The ozone profiles in MAM and SON have sharper increases than in other seasons above 13 km. The average ozone in the upper troposphere (above 10 km height) is highest in spring, particularly in March-April and lowest in autumn (SON). Measurements made over Hilo, Hawaii (19.4°N) have a maximum during spring in the free troposphere above 3 km [Cooper et al., 2011]. The present results also show that the highest ozone values in the free troposphere above Ahmedabad occur in spring. The lowest ozone in the 10-12 km range is observed in SON at both the locations. However, overall, ozone values are greater above Ahmedabad in all seasons, when compared with observations at Hilo.

Variation of ozone in the troposphere based on average monthly values at 200 m intervals using all balloon flights during 2003-2007 is shown in Figure 4b. Ozone mixing ratios are lowest below about 2 km during April to September. This is the period when the winds are from south-west, bringing air from the marine regions of the Indian Ocean and the Arabian Sea.

Higher ozone mixing ratios are observed from October to March below about 2 km. However, lower ozone levels are observed during these months between 3 and 5 km. In the mid-troposphere, ozone values as high as 70-80 ppbv are observed in May-June at 6-9 km. The two higher ozone spots seen in May at 6 and 8 km heights are caused by relatively higher ozone peaks observed on 30 May 2007 and 4 May 2005 respectively. The FLEXPART analysis indicated that these higher ozone containing air came from higher latitudes on these two days. Lower ozone in the upper troposphere above 10 km is observed during August to November. High ozone in the upper troposphere is observed throughout the year except during August to October. Stratospheric intrusions penetrate deeper into the troposphere during March- April.

The average seasonal profiles discussed above show little vertical variability. However, there is large variability in the vertical tropospheric ozone distribution from flight to flight. Figures 5a,b show individual ozone profiles on several days during different months of 2005. The annual average profile is also shown for comparison. Large variability occurs not only in the upper troposphere but throughout the troposphere. Figure 5a shows ozone profiles during March and May 2005. Surface level ozone was observed to be lowest (only about 6 ppbv) on 9 March, but ozone was highest above 11 km (greater than 100 ppbv at 11 km). On the contrary, ozone was highest (~ 65 ppbv) around 2 km on 16 March, but lowest (~30 ppbv) around 11 km. The ozone profile on 4 May shows very high ozone (~105 ppbv) around 8.5 km, while on 16 March it was only about 25 ppbv at the same altitude. Similar sharp peaks with values of 100 and 115 ppbv were observed at 6-9 km on 8 June, 2005 (Figure 5b). Such high ozone layers have been observed at other locations [Newell *et al.*, 1999; Lal *et al.*, 2013].

Figure 6 shows observed monthly average ozone at selected heights covering different regions of the troposphere. The variation of the monthly average tropospheric column ozone estimated

from the observed profiles are also shown for a comparison. Ozone mixing ratios at 0.5 km (average of values within  $\pm 0.5$  km) show large variation with decreasing ozone from 44 ppbv in January to a minimum of 18 ppbv in September. There is a sudden increase in ozone at this height in October with a maximum of 53 ppbv in November. The average ozone values at 4.5, 8.5 and 12.5 km show different patterns than that at 0.5 km. Ozone values at 4.5 and 8.5 km have maxima during April-May with lowest values in January. The variation at 12.5 km shows sharper changes but the maximum ozone (81 ppbv) is observed in early spring (March-April). Additionally, higher ozone is also seen in winter (December-January). The tropospheric ozone column (TOC) is greatest in April (~44 DU) and least (~34-35 DU) during July, August and September. Sharp increases in TOC are also observed from September to October, as at 0.5 km.

#### **4.3 Residence times of air parcels in different global regions**

The FLEXPART retroplume technique [Stohl *et al.*, 2003; Cooper *et al.*, 2005a; 2010] has been used to calculate residence times of air parcels above several regions including India, SE Asia, China, Japan-Korea, Central Asia, the Middle East, Africa, Europe, N. America and S. America (Figure 7).

Figures 8a,b,c,d show the average residence times of the retroplumes released from Ahmedabad over India, SE Asia, Central Asia, the Middle East, the Arabian Sea and other regions of the world for different seasons, expressed as the percent of the total global surface residence time for a retroplume over the previous 12 days. During winter (Figure 8a) in the lowest km of the troposphere (within the planetary boundary layer), the percent residence time over India is about 50%, but decreases sharply with altitude. The other major contributions below 4 km are from the Arabian Sea and the Middle East. The contribution from Africa

dominates above 4 km, albeit in the range of 20-30%. Other regions contribute in the range of 15-20% except East Asia which is less than 10% above about 8 km. The ozone distribution in this season, after the sharp increase in the first one km, decreases up to about 4 km. This is also the height where the residence time over India becomes much less and the contribution from Africa becomes dominant. In fact, ozone is lower than in any other season in the 3-8 km range but it is higher above 10 km than in other seasons, such as the summer monsoon and post-monsoon. The dip seen in the monsoon and post-monsoon seasons around 12 km is not seen in winter. This seems to be due to the dominance of air coming from the Africa.

The average residence time percentages for the pre-monsoonal spring season (March, April and May) are shown in Figure 8b. Compared to winter the contribution from India (25-35%) has increased in the entire troposphere except in the lowest one km. The contribution from the Arabian Sea (mostly in the range of 20-30%) has also increased as compared to winter. On the contrary, the contribution from Africa has decreased and it is less than 25% even in the 8-12 km region. Contributions from other regions have also decreased. Ozone levels have increased at all altitudes above 3 km as compared to winter. This change in residence times, particularly the increase in the contribution from India is associated with increased ozone levels above 3 km.

During the monsoon season (June, July and August), the percent residence time over India increases sharply above 2 km to approximately 55% in the 6-10 km range (Figure 8c). This is also the region of the troposphere with the highest ozone mixing ratios. The percent residence time over the Arabian Sea is greatest only below 2 km and decreases above this height. Above 8 km, the contribution from East Asia is the second greatest but only reaches 20%. This pattern

indicates a strong re-circulation of air above India during the summer monsoon that also extends to SE Asia, the Middle East, Central Asia and the Arabian Sea.

The percent residence times during the post-monsoon (fall) season (SON) are shown in Figure 8d. Residence times over India dominate throughout the troposphere. Residence times are about 55% in the lower 2 km, much greater than during the monsoon season, but above 4 km, the Indian residence times are much lower than during the monsoon season. The percent residence time over the Arabian Sea decreased to 25% below 3 km but increased (to 25%) above this height in comparison to the monsoon season. The vertical ozone distribution between the monsoon and fall (post-monsoon) seasons is correlated with the residence time above India. Below 4 km both ozone and the Indian residence time increase from the monsoon to the post-monsoon seasons, with the opposite effect above 4 km.

#### **4.4 Residence times over different regions**

The average monthly residence times are shown in Figure 9 for several regions. The residence time over India is always higher below 2 km except during the monsoon season, with maximum values occurring during September-December (note the colour scale, which is different than over the other regions). The residence time over India is also higher throughout the troposphere from mid-May to mid-October. Note that while the winds in the lower troposphere (<2 km) reach Ahmedabad directly from the Indian Ocean and the Arabian Sea during the peak monsoon period, the weak upper level winds allow air to reside over the Indian region during the previous 12 days. During this period, the retroplumes also show transport from East Asia in the mid-troposphere (6-12 km). The East Asian plume is also relatively stronger in the 7-12 km layer and during the July to September period (Figure 9), when the rains over Ahmedabad are heaviest.

350

351 Average ozone levels during the monsoon months (JJA) are lowest below about 3km height as  
352 the winds are directly from the Indian Ocean via the Arabian Sea. Even though peak ozone  
353 levels occur in May at 5-10 km, ozone remains high during the monsoon and fall months in  
354 this height range, while residence times are much higher for the Indian region and East Asian  
355 region. This may be due to higher levels of pollutants.

356

357 The residence time over the Arabian Sea is more-or-less higher in the lower troposphere  
358 throughout the year, mainly due to proximity to the western Indian region. The residence time  
359 over the Arabian Sea is higher during April to October below 2 km. However, there is a dip  
360 during July, when the transport pathway from the Indian Ocean touches the African east coast.  
361 Ozone is lower throughout this period in this height region. The residence time over this marine  
362 region is also higher at the beginning and end of the monsoon period.

363

364 March to May experiences hot and dry winds from the Middle East (Figure 9) below about 6  
365 km. This effect is also seen beyond October in the 2-10 km range. This transport pattern only  
366 corresponds to lower ozone mixing ratios. As mentioned earlier, July experiences transport  
367 from the east coast of Africa below about 2 km. Transport is also from this region above 4 km  
368 during October to May. The residence times of retroplumes during October to May above 4  
369 km is dominated by the African region. However, there is also transport from North America  
370 especially during March-May in the 4 to 8 km region above Ahmedabad.

371

#### 372 **4.5 Long range transport effects**

373 Many recent studies have documented inter-regional and inter-continental air pollution  
374 transport such as from Asia to North America [*Cooper et al.*, 2010; *Lin et al.*, 2012] and from



Asia to Europe [Lawrence and Lelieveld, 2010]. There is also evidence to show that pollutants from Europe, North Africa, etc., also reach East Asia [Newell and Evans, 2000; Naja and Akimoto, 2004] and in particular the south Asian region [Srivastava et al., 2011; Lal et al., 2013]. Transport of pollutants from India to the surrounding marine regions was well documented during INDOEX [Lelieveld et al., 2001] and other campaigns [Srivastava et al., 2011; Lal et al., 2013].

The FLEXPART retroplume analysis over Ahmedabad shows transport of air parcels from nearby regions or from as far away as North America depending upon altitude and season. Figure 10a shows the average transport pathways during winter (DJF), spring (MAM), monsoon (JJA) and post-monsoon/fall (SON) at 0-1 km, 7-8 km and 12-13 km. The corresponding average heights of the retroplumes during the 12 days prior to the release are shown in Figure 10b. Within the boundary layer (0-1 km) ozone over Ahmedabad is affected in winter mostly by regional transport from the northwest across India, Pakistan, Afghanistan, etc. (Figure 10a). However, in the upper troposphere during this season, ozone can be affected by transport from North Africa, the North Atlantic Ocean, the Central US and the North Pacific Ocean. The corresponding average height of the plumes during this season and during the past 12 days shows descending air from the free troposphere (4-5 km) down to the 0-1 km layer (Figure 10b). However, there is almost no change in the height of the retroplume in the mid-troposphere (7-8 km). The pattern in the 12-13 km layer shows a marginal lifting of the air masses. The ozone distribution in spring is affected by dynamics similar to winter at all heights, except that the transport patterns extend further to the west.

Transport characteristics during the monsoon are very different (Figures 10a,b). Ahmedabad is affected by monsoon winds in the 0-1 km range from the Indian Ocean/Arabian Sea via the

east coast of Africa and the western Gulf countries. The mid-troposphere is affected by transport from India, East Asia and to a small extent from North Africa. However, the upper troposphere over Ahmedabad is affected by convective transport from India, the Middle East and East Asia only. The closed region of recirculation is due to the persistent anticyclonic winds associated with the summer monsoon flow. As in the earlier two seasons, the vertical transport of the average retroplumes shows descent to the 0-1 km layer, marginal lifting to the 7-8 km layer and stronger convective lifting from below 8 km up to the 12-13 km layer (Figure 10b). In the monsoon season, ozone levels are lower in the upper troposphere compared to winter and spring. But the lowest ozone levels are observed during August-November than in any season at 10-14 km above sea level. These in situ observations are in contrast to other studies based on satellite data which show that the lowest ozone values at these altitudes occur during the Asian summer monsoon due to deep convection [Park *et al.*, 2007, 2009; Randel *et al.*, 2010].

The unique transport pattern during the summer monsoon also produces conditions most conducive for photochemical ozone production in the mid- and upper troposphere above India. Figure 11 shows the abundance of the FLEXPART anthropogenic NO<sub>x</sub> tracer above Ahmedabad. This passive tracer with a 12-day lifetime indicates that relatively fresh anthropogenic emissions are most common in the free troposphere during the summer monsoon. Approximately 80% of the NO<sub>x</sub> tracer in the upper troposphere is originated from the surface of India. This result suggests that future changes in Indian emissions would have their greatest impact on the chemical composition of the atmosphere above India during the summer monsoon, a phenomenon that deserves further research, both in terms of chemical transport modelling and in situ observations of chemistry and radiation.

The post-monsoon/fall season is the transition from monsoon to winter conditions and the transport characteristics also change. The vertical transport of the retroplumes at all three levels is similar to those in winter. Ozone levels are lowest above 9 km in this season.

#### **4.6 Stratosphere-Troposphere Exchange**

The stratosphere is a significant source of ozone for the middle and upper troposphere as a result of stratosphere-troposphere exchange processes in the extra-tropics [Stohl *et al.*, 2003]. This flux is greatest in spring [Crutzen, 1995 and references therein], and mainly associated with stratospheric intrusions into the troposphere that form filamentary structures that appear as laminae in ozone profiles [Holton *et al.*, 1995; Stohl *et al.*, 2003]. Stratosphere-to-troposphere transport has also been observed in the tropics involving the transport of stratospheric intrusions from mid-latitudes or wave breaking in the sub-tropics [Baray *et al.*, 1998; Cooper *et al.*, 2005b]. Satellite observations have revealed higher ozone in the upper troposphere above India due to transport from the stratosphere during winter and the pre-monsoon period [Fadnavis *et al.*, 2010]. Balloon-based measurements have shown stratospheric ozone intrusions in the mid- and upper troposphere above the Indian Ocean during February-March 1999 [Zachariasse *et al.*, 2001] and above the Arabian Sea during May, 2006 [Lal *et al.*, 2013] and over the central Himalayas [Ojha *et al.*, 2014].

Figure 12 shows the quantity of stratospheric ozone in the troposphere above Ahmedabad according to FLEXPART. The monthly values are averages corresponding to the times of the ozonesonde measurements during 2003-2007. These results show enhanced ozone in March, August and December in the upper troposphere. Modelled stratospheric contributions are located down to 10 km, with ozone values of about 15-20 ppbv. Extremely high ozone (about

150 ppbv) was observed on 11 April 2007 at about 11.5 km. FLEXPART indicated that this air parcel was transported from the Pacific Ocean via North Africa. It is interesting to note that even around 5-6 km, FLEXPART indicates stratospheric ozone intrusions during April-June with enhancements up to 15 ppbv. Ozone was observed to be more than 100 ppbv on 30 May 2007 at 6 km, with transport from the upper troposphere and lower stratosphere above the eastern US, followed by descent to Ahmedabad via the high latitude region of Europe.

*Livesey et al.* [2013] observed seasonally enhanced ozone at 215 hPa (~ 12 km height) over India during March-April using Microwave Limb Sounder (MLS) satellite data. We also observed these high ozone values above Ahmedabad, but in addition our ozone profiles demonstrate that the enhanced ozone during spring extends down to 6-9 km, a region of the troposphere not visible to MLS.

## **5. Summary and conclusions**

The vertical distribution of ozone was measured above Ahmedabad using ECC ozonesondes launched twice per month during May 2003 to July 2007, for a total of 83 soundings. The variability of ozone in the troposphere has been studied using these data. The tropospheric column content is at a maximum (44 DU) in April and at a minimum (35 DU) during the monsoon season (July to September). The maximum contribution to this total is associated with altitudes below 4 km. The seasonal average vertical profiles show different features in the three regions of the troposphere: i. below 4 km (lower troposphere), ii. between 4 and 10 km (middle troposphere) and iii. between 10 and 16 km (upper troposphere). In the lower troposphere ozone is greatest during winter (DJF) and lowest during the summer monsoon (JJA). But in the middle troposphere, ozone is at a maximum in spring (MAM) followed by JJA, and lowest in winter (DJF). In the upper troposphere, ozone is at a maximum in summer

and lowest in the fall (SON). Even though the seasonal ozone profiles do not show much variability, individual profiles show large variability in the middle and upper troposphere, where ozone ranges from 30 ppbv to 110 ppbv.

The FLEXPART retroplume technique was used to calculate residence times of air parcels over several regions such as India, SE Asia, China, Japan-Korea, Central Asia, Middle East, Africa, Europe, N. America and S. America. The residence times and locations of the plumes show very different characteristics. In the lower troposphere (particularly below 2 km) during the summer monsoon, transport is from the Indian Ocean and Arabian Sea via the east coast of Africa. But during winter, the transport pathway is across north-western India, Pakistan and Afghanistan. It is interesting to note that in the upper troposphere, the transport pathway is centred over the central Asia region during the summer monsoon but can circle the globe in the zonal direction during winter. This transport pattern can advect stratospheric ozone from higher latitudes to Ahmedabad.

High values of pollutants like CO and low values of ozone have been observed in the upper troposphere - lower stratosphere (UTLS) region during the summer monsoon above North Africa and the Middle East using satellite retrievals (AIRS and MLS) [Randel and Park, 2006; Park *et al.*, 2007, 2009]. These observations are believed to be due to convectively lifted air from the surface source regions during summer that becomes trapped in the anti-cyclonic winds in the upper troposphere. Since the convection over India is strong during the monsoon season, lower ozone in the upper troposphere during this season could be due to convective lofting of low ozone air from the lower troposphere.

We observe low ozone over Ahmedabad in the 10-14 km layer from July to November. As mentioned in the previous paragraph, we hypothesize that the low ozone in the UT is due to convective lofting of surface air that is depleted in ozone. Other satellite measurements based on TES retrievals show higher ozone in summer in the middle troposphere above North Africa, the Middle East and India [Worden *et al.*, 2009; Liu *et al.*, 2009, 2011]. They argue that this mid-tropospheric enhanced ozone in summer is due to long-range transport of ozone and local production due to enhanced pollutant levels. As mentioned earlier, we find higher ozone in the 6-9 km layer during April-June. Additionally, March-April ozone enhancements detected by MLS are verified here. FLEXPART indicates long range transport from North America, Africa and the Middle East to Ahmedabad for this season and altitude range. Hence, different altitudes and seasons have different transport and chemistry in the troposphere.

This is the first detailed analysis of ozone in the full troposphere above western India. These measurements will be useful for the validation of satellite retrievals and model simulations. While this data set gives a broader view of variability of ozone over Ahmedabad and the effects of transport and chemistry, there is a need to understand the various sources and photochemical processes using chemical transport models.

**Acknowledgements:** We thank PRL and ISRO GBP for encouraging and supporting this balloon program at PRL. SL is grateful to D. Kley and H. Smit for their help in the initial planning of this balloon sounding program at PRL. SL is also grateful to A. R. Ravishankara, former Director (now at Colorado State University) of the NOAA Earth System Research Laboratory's Chemical Sciences Division, Boulder, USA for supporting his stay there to initiate this analysis. We thank Shilpy Gupta, K. S. Modh, T. A. Rajesh and T. K. Sunilkumar for their support in conducting these balloon flights from Ahmedabad. We thank the

anonymous reviewers for their fruitful comments and suggestions, which have greatly improved the MS. We are also grateful to the Editor for his encouragement and support. The EDGARv4.1 global NO<sub>x</sub> emissions inventory was provided by European Commission, Joint Research Centre (JRC)/Netherlands Environmental Assessment Agency (PBL): Emission Database for Global Atmospheric Research (EDGAR), release version 4.1 <http://edgar.jrc.ec.europa.eu>, 2010. The international shipping NO<sub>x</sub> emission inventory was provided by James Corbett, University of Delaware. Fire NO<sub>x</sub> emissions are from the Global Fire Emissions Database version 3 (GFED3).

## References

- Akimoto H. (2003), Global Air Quality and Pollution, *Science* 302, 1717-1719.
- Baray, J., L. Baray, G. Ancellet, F. G. Taupin, M. Bessafi, S. Baldy, and P. Keckhut, (1998), Subtropical tropopause break as a possible stratospheric source of ozone in the tropical troposphere, *J. Atmos. Solar Terr. Phys.*, 60, 27–36.
- Barret B., E. L. Flochmoen, B. Sauvage, E. Pavelin, M. Matricardi, and J. P. Cammas (2011), The detection of post-monsoon tropospheric ozone variability over south Asia using IASI data, *Atmos. Chem. Phys. Discuss.*, 11, 10031–10068
- Beig, G., and V. Singh (2007), Trends in tropical tropospheric column ozone from satellite data and MOZART model, *Geophys. Res. Lett.*, 34, L17801, doi:10.1029/2007GL030460.
- Cooper, O. R., et al. (2005a), A springtime comparison of tropospheric ozone and transport pathways on the east and west coasts of the United States, *J. Geophys. Res.*, 110, D05S90, doi:10.1029/2004JD005183.
- Cooper, O. R., et al. (2005b), Direct transport of mid-latitude stratospheric ozone into the lower troposphere and marine boundary layer of the tropical Pacific Ocean, *J. Geophys. Res.*, 110, D23310, doi:10.1029/2005JD005783.

549 Cooper, O. R., et al. (2006), Large upper tropospheric ozone enhancements above  
 550 midlatitude North America during summer: In situ evidence from the IONS and  
 551 MOZAIC ozone measurement network, *J. Geophys. Res.*, 111, D24S05,  
 552 doi:10.1029/2006JD007306.

553 Cooper et al., (2010), Increasing springtime ozone mixing ratios in the free troposphere over  
 554 western North America, *Nature* 463, 344-348.

555 Cooper, O. R., et al. (2011), Measurement of western U.S. baseline ozone from the surface to  
 556 the tropopause and assessment of downwind impact regions, *J. Geophys. Res.*, 116,  
 557 D00V03, doi:10.1029/2011JD016095.

558 Corbett, J. J. and H. W. Koehler (2003), Updated emissions from ocean shipping, *J. Geophys.*  
 559 *Res.*, 108(D20), 4650, doi:10.1029/2003JD003751.

560 Crutzen P. J. (1995), Ozone in the troposphere in Composition, chemistry, and climate of the  
 561 atmosphere, Editor H. B. Singh, Van Norstrand Reinhold, New York. Dentener, F., T.  
 562 Keating, and H. Akimoto (Eds.) (2011), Hemispheric Transport of Air Pollution 2010:  
 563 Part A: Ozone and Particulate Matter, *Air Pollut. Stud*, vol. 17, U. N., New York.

564 Dentener, F., T. Keating, and H. Akimoto (Eds.) (2011), Hemispheric Transport of Air  
 565 Pollution 2010: Part A: Ozone and Particulate Matter, *Air Pollut. Stud*, vol. 17, U. N.,  
 566 New York. Emanuel K. A. (1994) Atmospheric convection, Oxford university press.

567 Fadnavis S., T. Chakraborty, and G. Beig (2010), Seasonal stratospheric intrusion of ozone in  
 568 the upper troposphere over India. *Ann. Geophys.*, 28, 2149–2159.

569 Fishman J., A. E. Wozniak, and J. K. Creilson (2003) Global distribution of tropospheric ozone  
 570 from satellite measurements using the empirically corrected tropospheric ozone  
 571 residual technique: Identification of the regional aspects of air pollution. *Atmos. Chem.*  
 572 *Phys.*, 3, 893–907.



573 Folkins I. and R. V. Martin, (2005), The vertical structure of tropical convection and its impact  
574 on the budgets of water vapor and ozone, *J. Atm. Sci.* 62, 1560

575 Gauss, M., et al. (2003), Radiative forcing in the 21st century due to ozone changes in the  
576 troposphere and the lower stratosphere. *J. Geophys. Res.* 108(D9),4292.  
577 doi:10.1029/2002JD002624

578 Gettelman, A., D. E. Kinnison, T. J. Dunkerton, and G. P. Brasseur (2004), Impact of monsoon  
579 circulations on the upper troposphere and lower stratosphere, *J. Geophys. Res.*, 109,  
580 D22101, doi:10.1029/2004JD004878.

581 Gurjar B. R., J. A. van Aardenne, J. Lelieveld, M. Mohan (2004), Emission estimates and  
582 trends (1990–2000) for megacity Delhi and implications, *Atmos. Env.* 38, 5663–5681

583 Holton J. R., P. H. Haynes, M. E. McIntyre, A. R. Douglass, R. B. Rood, L. Pfister (1995),  
584 Stratosphere-troposphere exchange, *Reviews of Geophysics*, 33, 403–439.

585 Intergovernmental Panel on Climate Change (IPCC) (2013), Working Group I contribution to  
586 the IPCC Fifth Assessment Report "Climate Change 2013: The Physical Science  
587 Basis", Final Draft Underlying Scientific-Technical Assessment, <http://www.ipcc.ch>

588 Kar, J., et al. (2004), Evidence of vertical transport of carbon monoxide from Measurements  
589 of Pollution in the Troposphere (MOPITT), *Geophys. Res. Lett.*, 31, L23105,  
590 doi:10.1029/2004GL021128.

591 Kley, D., H. G. J. Smit, H. Vomel, H. Grassl, V. Ramanathan, P. J. Crutzen, S. Williams, J.  
592 Meywerk, and S. J. Oltmans (1997), Tropospheric water vapour and ozone cross  
593 sections in a zonal plane over the central equatorial Pacific, *Q. J. R. Meteorol. Soc.*,  
594 123, 2009–2040.

595 Komhyr, W.D. and T. B. Harris (1971), Development of an ECC ozonesonde, NOAA Tech.  
596 Rep. ERL 200, APCL 18, , Boulder, CO USA.

Lacis, A. A., Wuebbles, D. J. and Logan, J. A., (1990), Radiative forcing by changes in the vertical distribution of ozone. *J. Geophys Res.* 95, 9971–9981.

Lal S., D. Chand, S. Venkataramani, K. S. Appu, M. Naja, P. K. Patra (2004), Trends in methane, and sulfure hexafluoride at a tropical coastal site, Thumba (8.6N, 77E), in India, *Atmos. Env.* 38(8), 1145-1151.

Lal S., S. Venkataramani, S. Srivastava, S. Gupta, C. Mallik, M. Naja, T. Sarangi, Y. B. Acharya and X. Liu (2013), Transport effects on the vertical distribution of tropospheric ozone over the tropical marine regions surrounding India , *J. Geophys. Res.*, 118, doi:10.1002/jgrd.50180.

Lawrence, M. G., and J. Lelieveld (2010), Atmospheric pollutant outflow from southern Asia: A review, *Atmos. Chem. Phys.*, 10, 11,017–11,096, doi:10.5194/acp-10-11017-2010.

Lelieveld, J. et al. (2001), The Indian Ocean Experiment: Widespread Air Pollution from South and Southeast Asia, *Science*, 291, 1031–1036.

Lelieveld et al. (2002), Global Air Pollution Crossroads over the Mediterranean, *Science* 25 October 2002: 794-799. DOI:10.1126/science.1075457

Lin, M., et al. (2012), Transport of Asian ozone pollution into surface air over the western United States in spring, *J. Geophys Res.*, 117, D00V07, doi:10.1029/2011JD016961

Liu, H., D. J. Jacob, I. Bey, R. M. Yantosca, B. N. Duncan, and G. W. Sachse (2003), Transport pathways for Asian pollution outflow over the Pacific: Interannual and seasonal variations, *J. Geophys. Res.*, 108(D20), 8786, doi:10.1029/2002JD003102.

Liu, J. J., D. B. A. Jones, J. R. Worden, D. Noone, M. Parrington, and J. Kar (2009), Analysis of the summertime build up of tropospheric ozone abundances over the Middle East and North Africa as observed by the Tropospheric Emission Spectrometer instrument, *J. Geophys. Res.*, 114, D05304, doi:10.1029/2008JD010993.

621 Liu, J. J., D. B. A. Jones, S. Zhang, and J. Kar (2011), Influence of interannual variations in  
622 transport on summertime abundances of ozone over the Middle East, *J. Geophys. Res.*,  
623 116, D20310, doi:10.1029/2011JD016188.

624 Livesey N. J., J. A. Logan, M. L. Santee, J. W. Waters, R. M. Doherty, W. G. Read, L.  
625 Froidevaux, and J. H. Jiang, (2013), Interrelated variations of O<sub>3</sub>, CO and deep  
626 convection in the tropical/subtropical upper troposphere observed by the Aura  
627 Microwave Limb Sounder (MLS) during 2004–2011, *Atmos. Chem. Phys.*, 13, 579–  
628 598.

629 Monks, P. S., et al. (2009), Atmospheric Composition Change – Global and Regional Air  
630 Quality, *Atmos. Environ.*, 43, 5268-5350.

631 Naja and Akimoto (2004), Contribution of regional pollution and long-range transport to the  
632 Asia-Pacific region: Analysis of long-term ozonesonde data over Japan, *J. Geophys.*  
633 *Res.*, 109, D21306, doi:10.1029/2004JD004687.

634 Newell, R., and M. Evans (2000), Seasonal changes in pollutant transport to the North  
635 Pacific: The relative importance of Asian and European sources, *Geophys. Res. Lett.*,  
636 27, 2509– 2512.

637 Newell R. E., V. Thouret, J. Y. N. Cho, P. Stoller, A. Marenco and H.G. Smit (1999), Ubiquity  
638 of quasi-horizontal layers in the troposphere, *Nature*, 398, 316-319.

639 Ohara, T., H. Akimoto, J. Kurokawa, et al., (2007), Asian emission inventory for anthropogenic  
640 emission sources during the period 1980–2020. *Atmos. Chem. Phys.*, 7, 4419–4444.

641 Ojha, N., M. Naja, T Sarangi, R Kumar, P Bhardwaj, S Lal, S Venkataramani, R Sagar, A  
642 Kumar, HC Chandola, (2014), On the processes influencing the vertical distribution of  
643 ozone over the central Himalayas: Analysis of yearlong ozonesonde observations,  
644 *Atmospheric Environment*, 88, 201-211.

645 Olivier, J. G. J., van Aardenne, J. A., Dentener, F., Pagliari, V., Ganzeveld, L. N., and J. A.  
 646 H.W., Peters (2005) Recent trends in global greenhouse gas emissions: regional trends  
 647 1970–2000 and spatial distribution of key sources in 2000, *Environ. Sci.*, 2, 81–99,  
 648 doi:10.1080/15693430500400345.

649 Park, M., W. J. Randel, A. Gettelman, S. T. Massie, and J. H. Jiang (2007), Transport above  
 650 the Asian summer monsoon anticyclone inferred from Aura Microwave Limb Sounder  
 651 tracers, *J. Geophys. Res.*, 112, D16309, doi:10.1029/2006JD008294.

652 Park, M., W. J. Randel, L. K. Emmons, and N. J. Livesey (2009), Transport pathways of carbon  
 653 monoxide in the Asian summer monsoon diagnosed from Model of Ozone and Related  
 654 Tracers (MOZART), *J. Geophys. Res.*, 114, D08303, doi:10.1029/2008JD010621.

655 Randel, W. J., and M. Park (2006), Deep convective influence on the Asian summer monsoon  
 656 anticyclone and associated tracer variability observed with Atmospheric Infrared  
 657 Sounder (AIRS), *J. Geophys. Res.*, 111, D12314, doi:10.1029/2005JD006490.

658 Randel W. J., et al. (2010), Asian Monsoon Transport of Pollution to the Stratosphere, *Science*  
 659 328, 611; DOI: 10.1126/science.1182274

660 Ravishankara A. R., J. P. Dawson, D. A. Winner (2012), New Directions: Adapting air quality  
 661 management to climate change: A must for planning, *Atmos. Env.* 50, 387–389

662 Saraf N. and G. Beig (2004), Long-term trends in tropospheric ozone over the Indian tropical  
 663 region. *Geophys. Res. Lett.*, 31, L05101, doi:10.1029/2003GL018516.

664 Smit, H. G. J., et al. (2007), Assessment of the performance of ECC-ozonesondes under quasi-  
 665 flight conditions in the environmental simulation chamber: Insights from the Juelich  
 666 Ozone Sonde Intercomparison Experiment (JOSIE), *J. Geophys. Res.*, 112, D19306,  
 667 doi:10.1029/2006JD007308.

668 Srivastava S., S. Lal S. Venkataramani, S. Gupta, and Y. B. Acharya (2011), Vertical  
 669 distribution of ozone in the lower troposphere over the Bay of Bengal and the Arabian

Sea during ICARB-2006: Effects of continental outflow, J. Geophys. Res.  
doi:10.1029/2010JD015298.

Srivastava S., S. Lal, M. Naja, S. Venkataramani and S. Gupta (2012), Influences of regional  
pollution and long range transport to western India: Analysis of ozonesonde data,  
Atmos. Env. 47, 174-182

Stevenson et al. (2012), Tropospheric ozone changes, radiative forcing and attribution to  
emissions in the Atmospheric Chemistry and Climate Model Inter-comparison Project  
(ACCMIP), Atmos. Chem. Phys. Discuss., 12, 26047–26097.

Stohl, A., et al. (2003), Stratosphere-troposphere exchange: A review, and what we have  
learned from STACCATO, J. Geophys. Res. 108, NO. D12, 8516,  
doi:10.1029/2002JD002490.

Stohl, A., C. Forster, S. Eckhardt, N. Spichtinger, H. Huntrieser, J. Heland, H. Schlager, H.  
Aufmhoff, F. Arnold, and O. Cooper (2003), A backward modeling study of  
intercontinental pollution transport using aircraft measurements, J. Geophys. Res.,  
108(D12), 4370, doi:10.1029/ 2002JD002862.

Stohl, A., C. Forster, A. Frank, P. Seibert, and G. Wotowa (2005), Technical note: The  
Lagrangian particle dispersion model FLEXPART version 6.2, Atmos. Chem. Phys., 5,  
2461–2474.

Streets, D.G., Bond, T.C., Carmichael, G.R., Fernandes, S.D., Fu, Q., He, D., Klimont, Z.,  
Nelson, S.M., Tsai, N.Y., Wang, M.Q., Woo, J., Yarber, K.F., (2003). An inventory  
of gaseous and primary aerosol emissions in Asia in the year 2000. J. Geophys. Res.  
108, 8809. doi:10.1029/2002JD003093. The Royal Society (2008), Ground-level  
Ozone in the 21st century: Future Trends, Impacts and Policy Implications, Royal  
Society policy document 15/08, RS1276,  
[http://royalsociety.org/Report\\_WF.aspx?pageid57924&terms5ground-level1ozone](http://royalsociety.org/Report_WF.aspx?pageid57924&terms5ground-level1ozone)

The Royal Society (2008), Ground-level Ozone in the 21st century: Future Trends, Impacts and Policy Implications, Royal Society policy document 15/08, RS1276, [http://royalsociety.org/Report\\_WF.aspx?pageid57924&terms5ground-level1ozone](http://royalsociety.org/Report_WF.aspx?pageid57924&terms5ground-level1ozone)

van der Werf, G. R. et al., (2010), Global fire emissions and the contribution of deforestation, savanna, forest, agricultural, and peat fires (1997-2009), *Atmos. Chem. Phys.*, 10, 11707-11735, doi:10.5194/acp-10-11707-2010.

Wild, O., M.J. Prather, H. Akimoto, J.K. Sundet, I.S.A. Isaksen, J.H. Crawford, D.D. Davis, M.A. Avery, Y. Kondo, G.W. Sachse, and S.T. Sandholm (2004), CTM Ozone Simulations for Spring 2001 over the Western Pacific: Regional ozone production and its global impacts, *J. Geophys. Res.*, 109, D15S02, doi:10.1029/2003JD004041.

Worden, J. et al., (2009), Observed vertical distribution of tropospheric ozone during the Asian summer time monsoon. *J. Geophys. Res.*, 114, D13304, doi:1029/2008JD010560

Zachariasse, M., H. Smit, P. van Velthoven, and H. Kelder (2001), Cross-tropopause and interhemispheric transports into the tropical free troposphere over the Indian Ocean, *J. Geophys. Res.*, 106(D22), 28441-28452.

# **Figure Captions:**

Figure 1: Average streamlines based on NCEP reanalysis data during winter (DJF), spring (MAM), monsoon (JJA) and fall (SON) seasons at 925, 500 and 200 hPa. The color bar code at the bottom is wind speed ( $\text{ms}^{-1}$ ).

Figure 2: Ozone, temperature and relative humidity profiles as observed from a balloon ascent on 25 June, 2003 above Ahmedabad.

Figure 3: (a) Average temperature, (b) relative humidity during different months and (c) average seasonal profiles of both, observed from the balloon ascents above Ahmedabad during 2003-2007.

Figure 4: (a) Average ozone mixing ratios (ppbv) during different seasons and (b) during different months observed from the balloon ascents above Ahmedabad during 2003-2007.

Figure 5: (a) Ozone profiles observed above Ahmedabad on different dates during March-May 2005 and (b) during Jun-August 2005, along with the annual average profile.

Figure 6: Average ozone during different months and at different heights based on all the balloon ascents made over Ahmedabad during 2003-2007. Variations in the monthly average tropospheric ozone columns are shown.

Figure 7: Example of a FLEXPART retroplume released from 100 m above mean sea level (amsl) at Ahmedabad, 4:00 UTC, 27 January, 2005. Shown are the retroplume pathway throughout the entire atmospheric column (top left), and only within the 300 m footprint layer (top right). The center of the 12-day retroplume is denoted by the white back trajectory with black dots indicating the mean location every 24-hours and white labels indicating every second day. Magenta boxes outline the regions for which NO<sub>x</sub> emissions are totaled. Also shown are the 2x2 degree EDGAR NO<sub>x</sub> emission inventory (center left) and the quantity of NO<sub>x</sub> emitted into the retroplume from each of the regions of interest (center right). Similarly, the emission inventory and NO<sub>x</sub> emitted into the retroplume at 0.5x0.5 degree resolution across South Asia are shown at bottom left and bottom right, respectively.

Figure 8: Percent residence times over different regions and for different seasons using the average FLEXPART model results for all the balloon flights conducted from Ahmedabad during 2003-2007. Average ozone profiles for each season are also shown.

Figure 9: Monthly average residence times (kSec) over major regions using the FLEXPART model results for all the balloon flights conducted from Ahmedabad during 2003-2007. Please note different scale used for India.

Figure 10: Composite diagrams showing FLEXPART 12-day retroplumes for 0-1 km (Column-1), 7-8 km (Column-2) and 12-13 km (Column-3) and for Dec-Jan-Feb (Row-1), Mar-Apr-May (Row-2), Jun-Jul-Aug (Row-3) and Sep-Oct-Nov (Row-4). Panel a shows transport pathways while Panel b shows average vertical movement of the retroplumes during the 12 days prior to release. Retroplumes correspond to the launch times of all balloon ascents during the respective season.

Figure 11: Estimated  $\text{NO}_x$  (ppbv) over Ahmedabad using the FLEXPART model.

Figure 12: Monthly average contribution of ozone from the stratosphere based on FLEXPART model calculations.



769

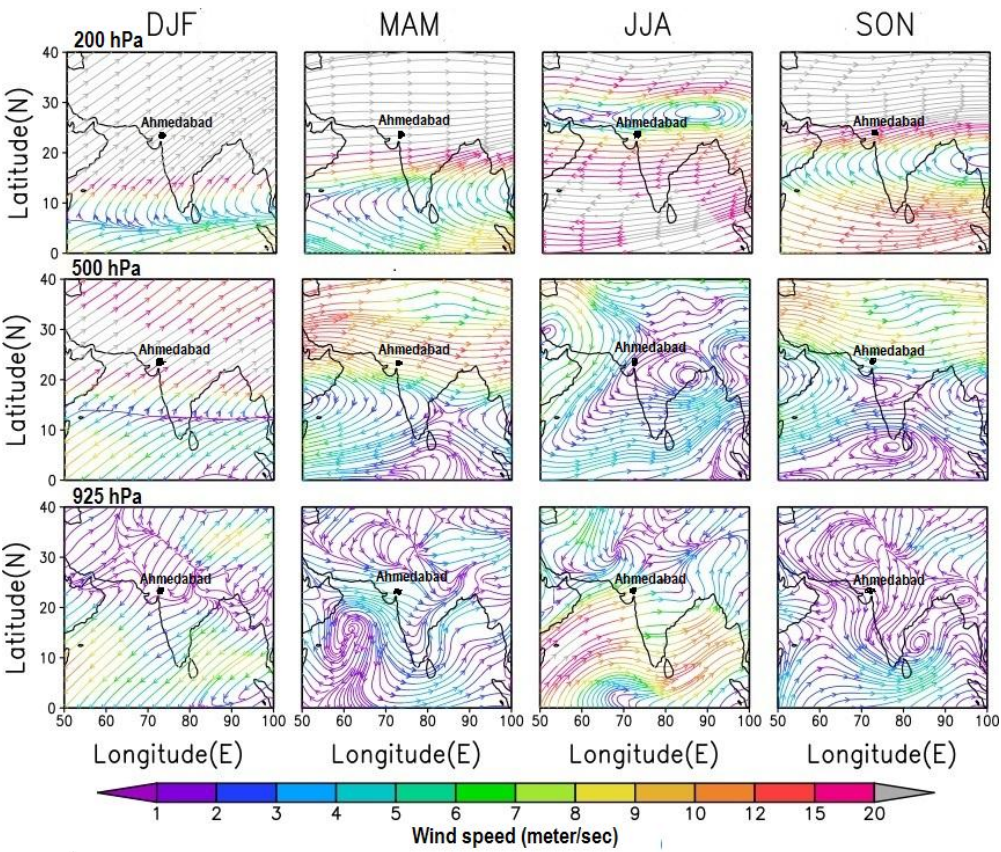
770

771

772

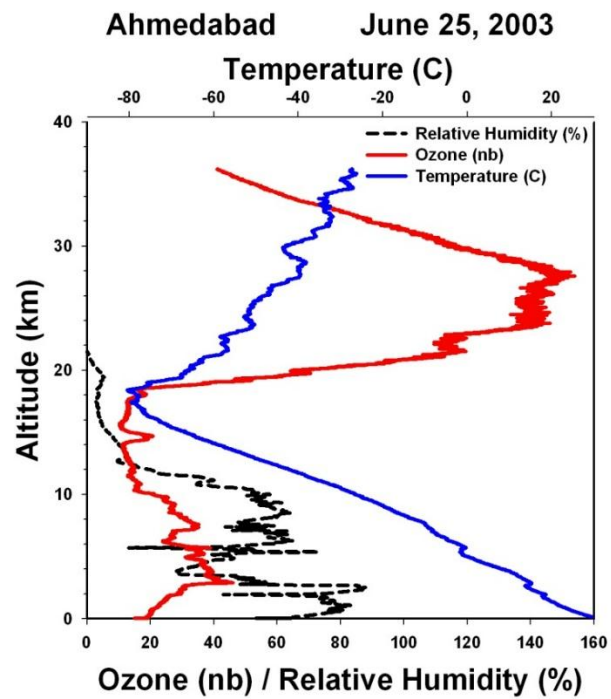
773 **Figures:**

774 **Figure 1:**



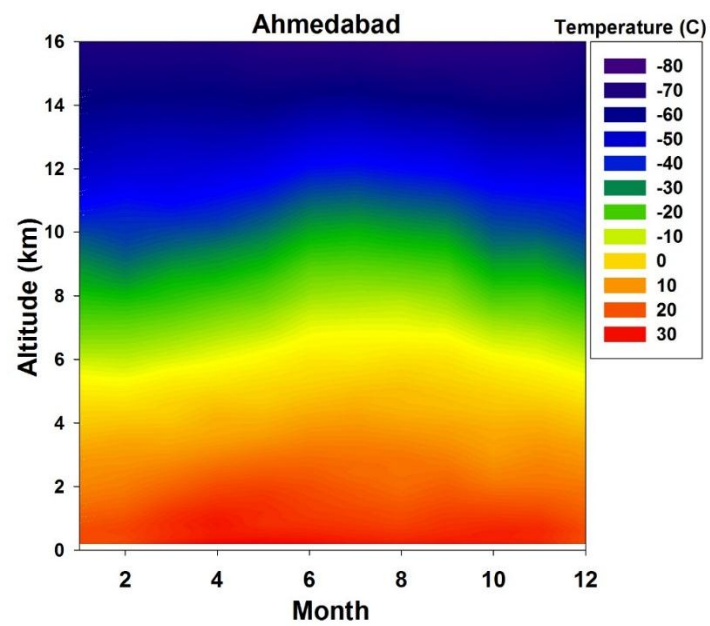
775

776 **Figure 2:**



777

778 **Figure 3a:**



779

780 **Figure 3b:**

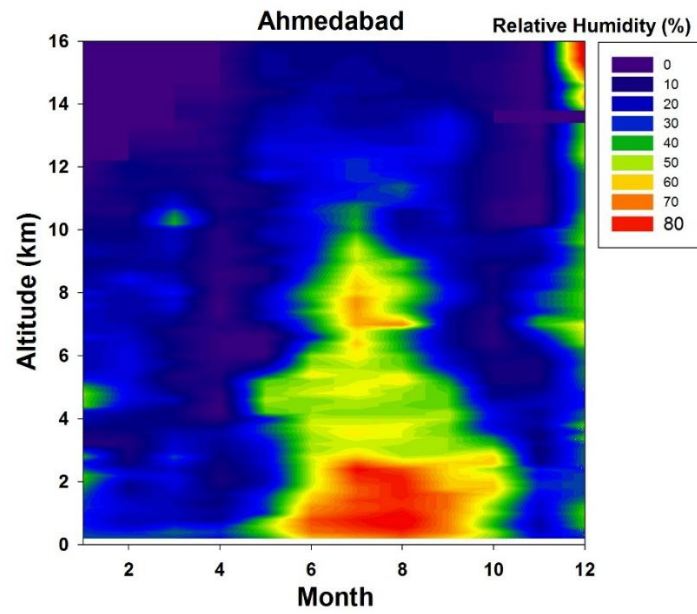


**Figure 3c:**

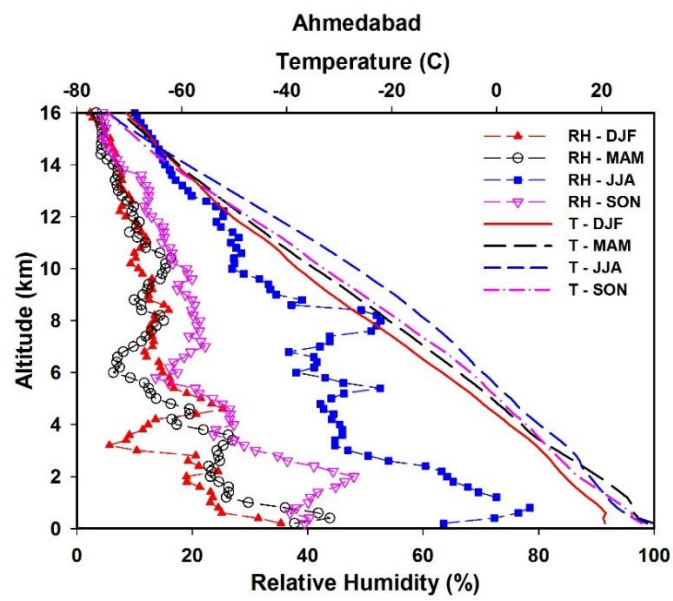


**Figure 4a:**

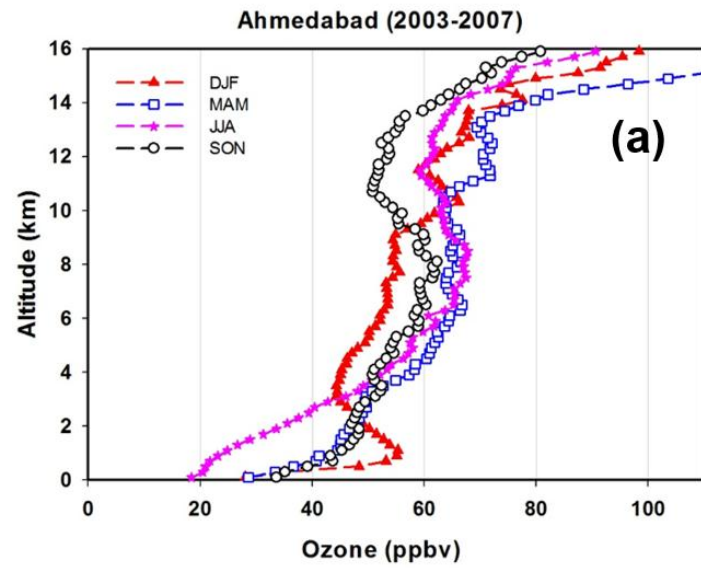
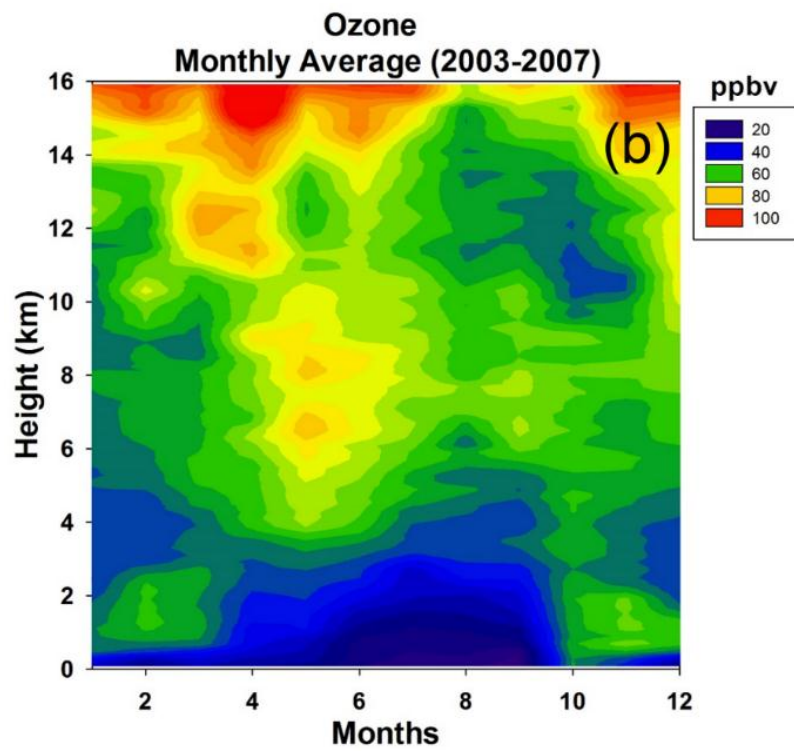


**Figure 4b:**



799

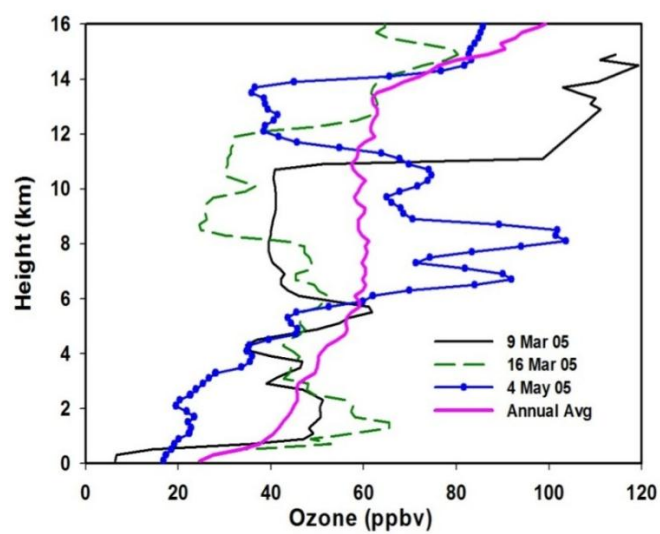
800

801

802

803

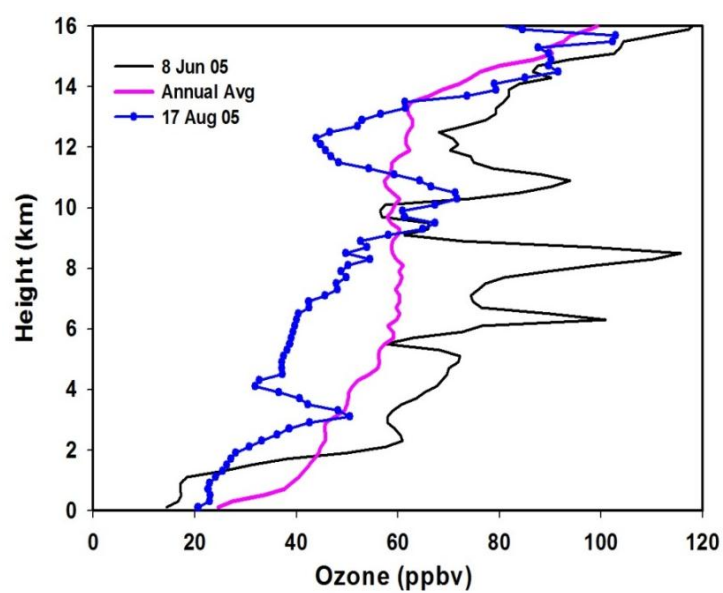
804 **Figure 5a:**



805

806 **Figure 5b:**

807



808



Figure 6:

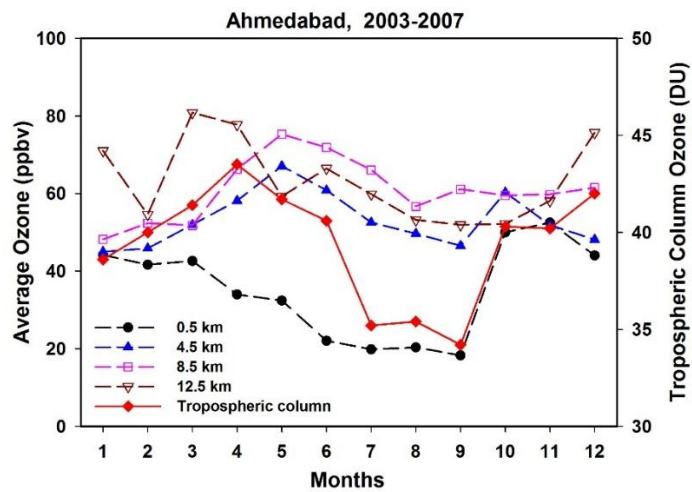
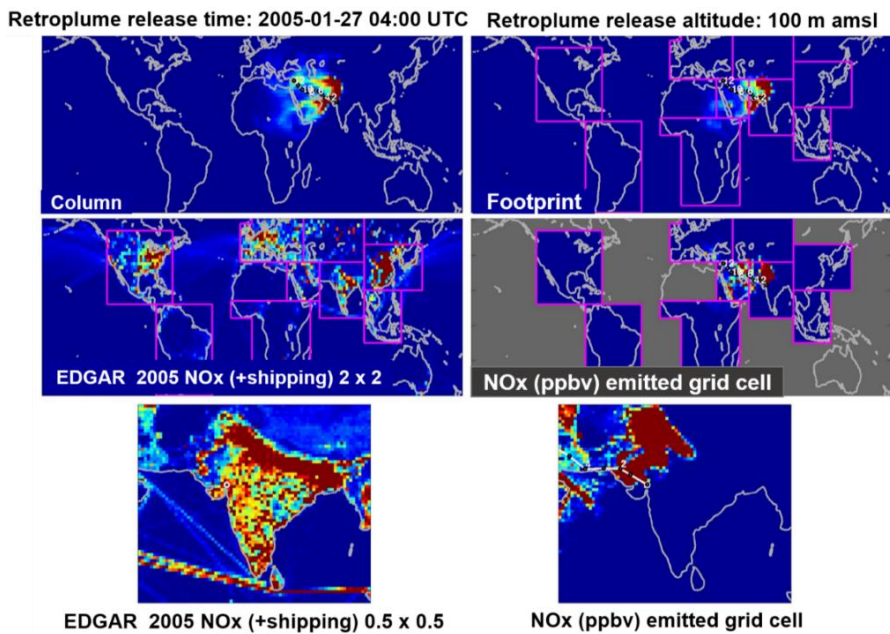
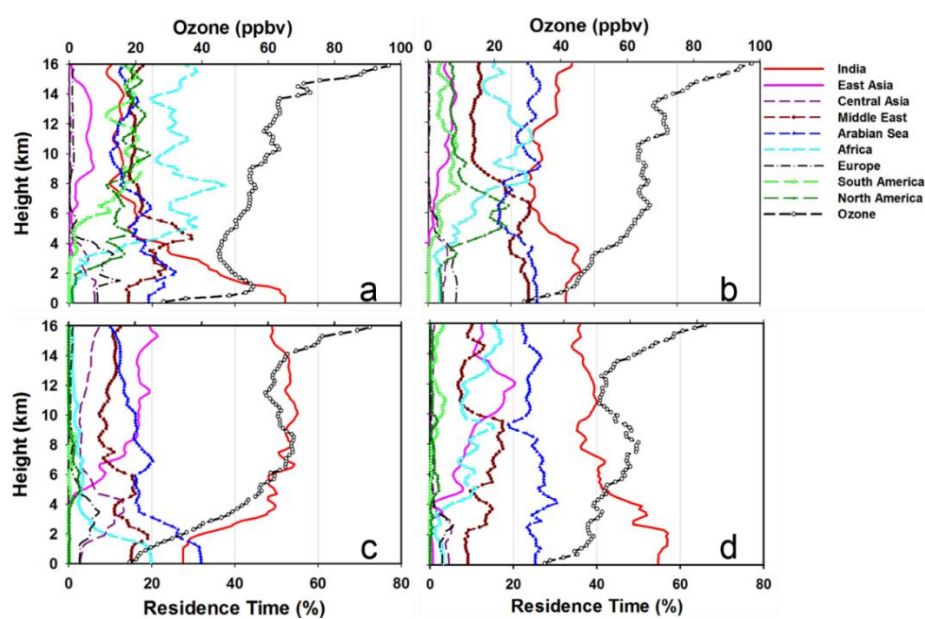


Figure 7:



820 **Figure 8:**



821

822

823

824

825

826

827 **Figure 9:**

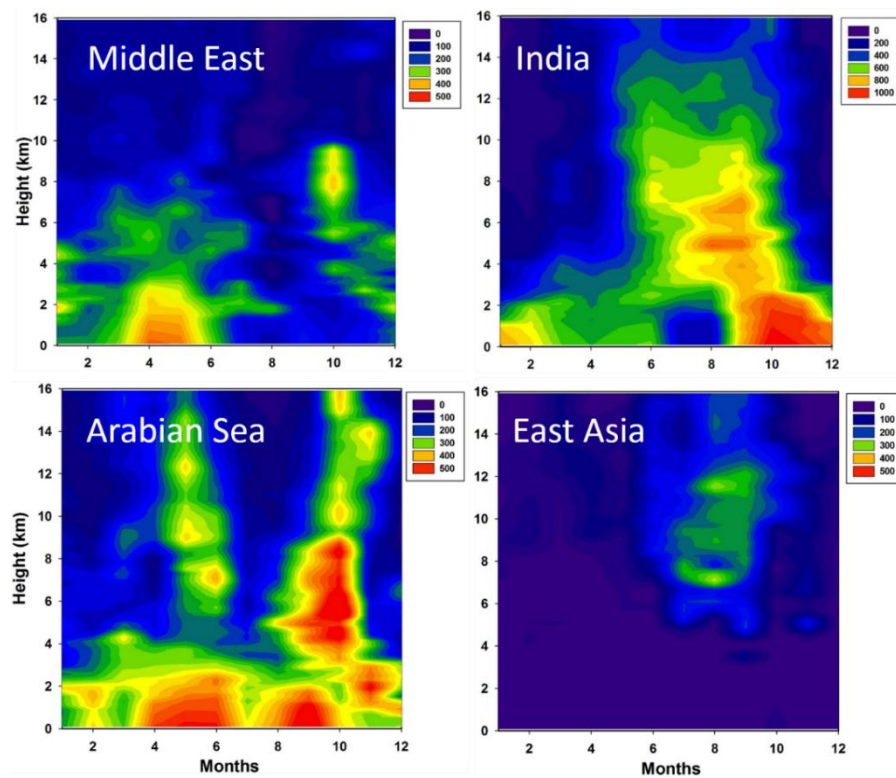
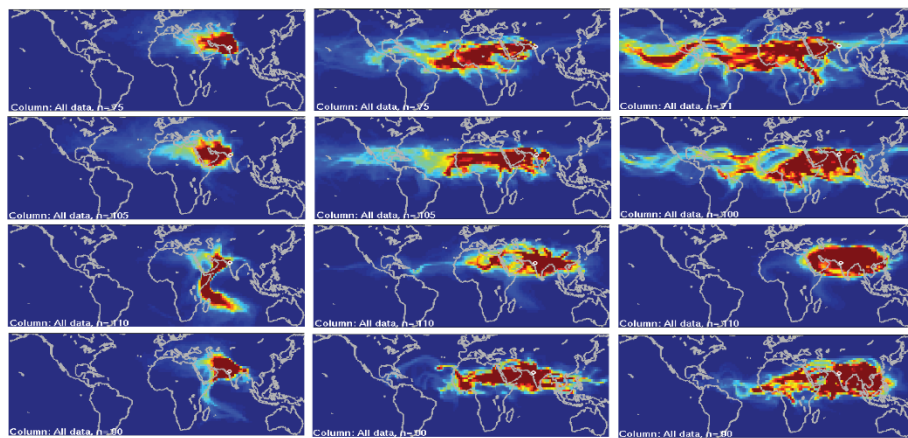
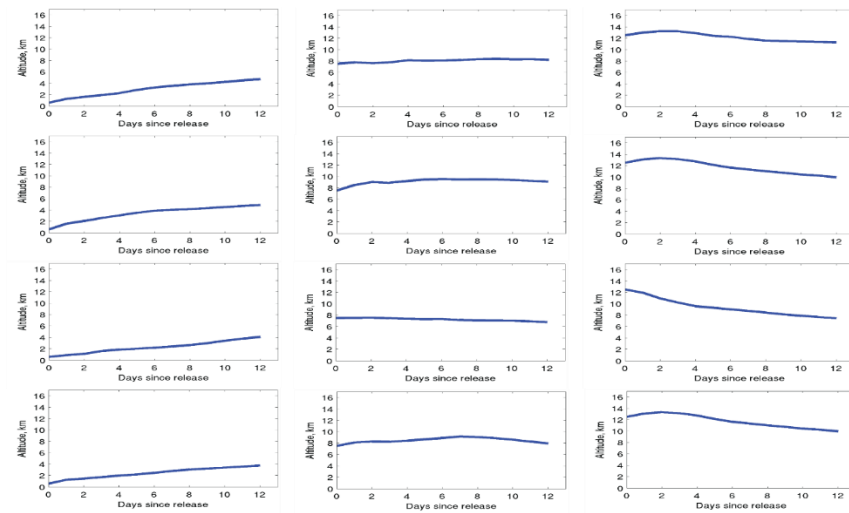


**Figure 10 a:**



Row 1: Dec-Jan-Feb, 0-1 km, 7-8 km, 12-13 km  
 Row 2: Mar-Apr-May, 0-1 km, 7-8 km, 12-13 km  
 Row 3: Jun-Jul-Aug, 0-1 km, 7-8 km, 12-13 km  
 Row 4: Sep-Oct-Nov, 0-1 km, 7-8 km, 12-13 km





Row 1: Dec-Jan-Feb, 0-1 km, 7-8 km, 12-13 km  
 Row 2: Mar-Apr-May, 0-1 km, 7-8 km, 12-13 km  
 Row 3: Jun-Jul-Aug, 0-1 km, 7-8 km, 12-13 km  
 Row 4: Sep-Oct-Nov, 0-1 km, 7-8 km, 12-13 km

**Figure 11:**

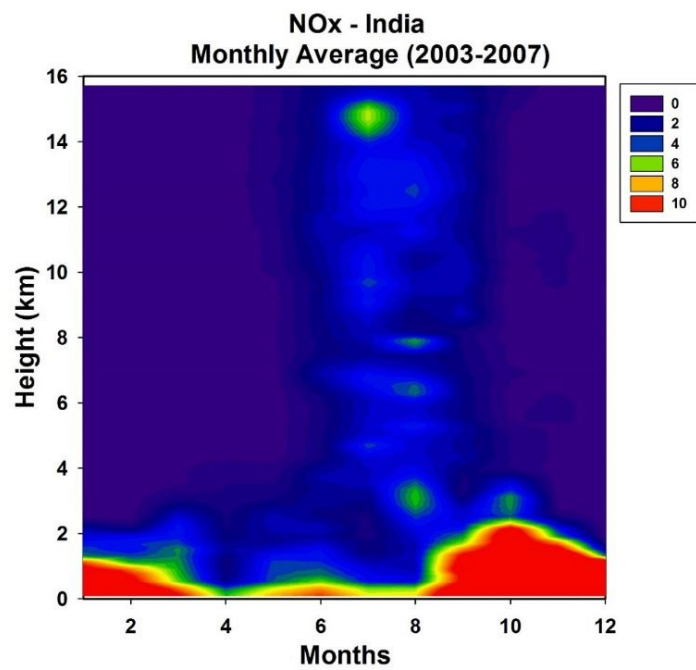
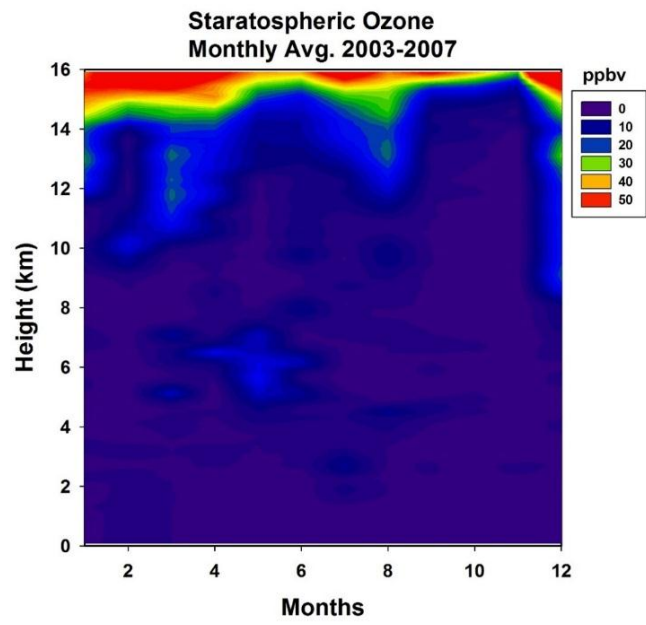


**Figure 12:**



845

846

847

848

849

850

851

852

853